 CMC, vol.27, no.3, pp.189-210, 2012

A Computational Approach to Estimating a Lubricating Layer in Concrete Pumping

Seon Doo Jo[1], Chan Kyu Park[2], Jae Hong Jeong[2]
Seung Hoon Lee[2] and Seung Hee Kwon[3]

Abstract: When concrete is being pumped, a lubricating layer forms at the interface of the inner concrete and the wall of the pipe. The lubricating layer is one of the most dominant factors in determining the pumping capability, yet no study has endeavored to quantitatively estimate the thickness and rheological properties of the layer. Recently, there has been a growing demand for large-scale construction under extreme conditions, such as high-rise buildings and super-long span bridges. This demand has heightened the need for more accurate predictions of pumpability.

A possible mechanism that contributes to the formation of the lubricating layer is shear-induced particle migration. That is, particles of suspension in the shear flow move from a region with a higher shear rate to a region with a lower shear rate. This study uses computational fluid dynamics to analyze the pipe flow of concrete under conditions of shear-induced particle migration. The analysis shows how the particle distribution as well as the plastic viscosity and yield stress vary throughout a particular cross section. The analysis results are used to estimate the thickness and rheological properties of the layer.

Keywords: lubricating layer, slip layer, concrete pumping, prediction, shear-induced particle migration, rheology, thickness, viscosity, yield stress.

1 Introduction

The process of designing concrete structures requires considerable effort to ensure the structures are safe, serviceable and durable. Specifically, finite element anal-

[1] Department of Civil and Environmental Engineering, Myongji University, San 38-2, Namdong, Cheoin-gu, Yongin, Gyeonggi-do, 449-728, South Korea

[2] Construction Technology Research Institute, Samsung C&T Corporation, 23rd Floor, Samsung Corporation Building, 1312-20, Seocho-2Dong, Seocho-gu, Seoul, 137-857, South Korea

[3] Corresponding author. Tel.: +82 (31) 330-6418; Fax: +82 (31) 336-9705; E-mail: kwon08@mju.ac.kr

ysis should be used to assess the structures in terms of the following factors: the number of code provisions for failure, thermal stress, cracking, long-term deformation caused by creep and shrinkage, degradation of concrete and corrosion of reinforcement due to chemical attacks, and even a coupling effect of these factors [Nghia, Chu and Kim (2010); Chun, Lee and Oh (2010); Ferretti and Leo (2008); Kwon and Shah (2008); Kwon, Zhao and Shah (2008); Zhao, Kwon and Shah (2008); Charkrabarty and Cargin (2008)]. The structural design is based on quantitative predictions of structural behavior and performance. Naturally, the structures should be well constructed so that they can perform the targeted or predicted structural functionalities. In other words, the construction itself is as important as the design of the structures. To date, however, the focus of construction has been on qualitative standards. For example, the estimated workability of many sites is often based exclusively on a simple test, such as a slump test or a slump flow test. Quantitative predictions are rare in real construction processes, such as pumping, casting and compaction, formwork pressure, partial or full segregation, and the distribution and orientation of fibers in fiber-reinforced cementitious materials. Recently, however, researchers have stepped up their attempts to quantitatively predict the rheological behavior of fresh concrete and to apply the prediction results to real construction processes [Kwon, Phung, Park, Kim and Shah (2011); Kim, Beacraft, Kwon and Shah (2011); Kwon, Shah, Phung, Kim and Lee (2010)]. More extensive predictive capabilities are likely to be needed for the construction processes in the near future.

Concrete pumping is a major issue in the construction of high-rise buildings, long-span bridges, and other structures that require long-distance transport of concrete. For example, knowledge of the pumping flow rate (that is, the amount of concrete transported per hour) is required for the construction of a high-rise building of several hundred meters. This variable is useful for controlling the casting speed and for determining the total duration of the construction period, which is directly related to the construction cost.

A study of Kaplan, Larrard and Sedran (2005) on predicting the pumping speed showed that the slip layer or lubricating layer that forms near the interface of the concrete and the inner wall of the pipe is a dominant factor in facilitating pumping. They developed a test instrument called a tribometer to measure the friction stress at the wall of the pipe, and they assumed the layer has a zero thickness. Other studies have suggested different types of tribometers and confirmed the presence of the slip layer [Ngo, Bennacer and Cussigh (2010); Chapdelaine (2007)]. In reality, however, the layer has a finite thickness and the rheological properties vary within the thickness. Currently, there is no way to directly measure the thickness of the lubricating layer or to experimentally determine how the rheological properties of the layer vary near the wall.

The objective of this study is to use numerical analysis to estimate the thickness and rheological properties of a lubricating layer. The first step was to examine whether the pumping could be predicted from a correlation of the flow rate and the rheological properties (specifically the plastic viscosity and yield stress); the values of these factors were measured at a real site as well as in a mock test [Sohn, Lee and Lee (2010)], and the measured data is used to ensure the necessity of estimating the lubricating layer through the numerical analysis. Numerical analysis was performed to estimate the lubricating layer considering shear-induced particle migration(SIPM) [Phillips, Armstrong and Brown (1992)] which was considered as a formative mechanism for the formation of the layer. A parametric study was undertaken to understand the effects of changes to the mix proportions, the particle size, the pumping pressure, the diameter of the pipe, and the rheological properties of concrete on the formation of the lubricating layer. The subsequent results on the particle distributions, the profiles of the plastic viscosity and the yield stress, the profiles of the shear rate and the velocity over a cross section of the pipe were used to quantitatively estimate the thickness and rheological properties of the lubricating layer.

2 Use of the rheological properties of concrete to predict pumping

For the construction of the world's highest building, the Burj Khalifa, at Dubai in 2005, concrete was pumped to the a world record height of 600 m. The plastic viscosity and yield stress of the concrete were measured with a rheometer immediately before the pumping began at the site; measurements were also taken of the flow rate and the pumping pressure. In 2009, as shown in Fig. 1, pumping tests over a distance of 1 km were performed in Korea [Sohn, Lee and Lee (2010)]. In the mock-up test, measurements were taken of flow rate, the pumping pressure at the inlet, and the rheological properties of the concrete prior to the pumping. Table 1 shows the values measured at both sites.

For the calculation of the flow rate, the measured plastic viscosity and yield stress were applied to the following equation, which is known as the Buckingham-Reiner equation [Tattersall and Banfill (1983)]:

$$Q = \frac{\pi a^4}{8\mu l}\left(P_i - \frac{4}{3}P_0 + \frac{P_0^4}{3P_i^3}\right), \quad P_o = \frac{2l\tau_0}{a}, \tag{1}$$

where Q is the flow rate, a is the radius of the pipe,l is the total length of the pipe, P_i is the inlet pressure, P_0 is the minimum pressure at which the flow begins, and μ and τ_0 are the plastic viscosity and yield stress in the Bingham fluid model, respectively.

Figure 1: A mock test over a distance of 1 km

Table 1 lists the flow rates that are derived from the measured rheological properties and compares these rates with the measured flow rates. The calculated flow rates are 10% to 40% of the measured flow rates, which indicates that the lubricating layer has much lower plastic viscosity and yield stress than the inner concrete near the wall of the pipe.

Table 1: Measured rheological properties, inlet pressures and flow rates of real pumping and the calculated flow rates

Mixes		Rheological properties		Inlet pressure (Bar)	Pipe		Flow rate (m^3/h)		
		Plastic viscosity (Pa·s)	Yield stress (Pa)		*Pipe length (m)	Radius (mm)	Measured (M)	Calculated (C)	C/M (%)
Burj Khalifa at Dubai (2005)	B1	44.1	0.1	171	83 (H) + 576 (V) = 659	75	21.3	7.9	37
	B2	73.6	29.4	180			21.8	5.1	23
	B3	70.5	32.5	179			18.8	5.1	27
	B4	75.5	29.3	176			19.4	4.5	23
Mock-up test in Korea (2009)	K1	107.0	0.1	107	400 (H)	62.5	18.9	5.4	29
	K2	71.9	0.1	124			31.4	9.3	30
	K3	49.3	0.1	88	700 (H)		23.7	2.8	12
	K4	143.0	0.1	120			11.9	2.6	22
	K5	96.0	0.1	178	1000 (H)		29.1	12.5	43
	K6	126.0	0.1	181			12.7	3.1	24
	K7	71.4	0.1	171			18.6	5.2	28

*Pipe length = H (horizontal length) + V (vertical length)

The real flow rates cannot be predicted without considering the effect of the lubricating layer. Nevertheless, it needs to examine if the rheological properties and the flow rates can be correlated or not. The left graph in Fig. 2 shows that the measured yield stress is not related to the flow rate per unit of pressure. The right graph, on the other hand, suggests that the flow rate seems to increase as the plastic viscosity decreases, though the deviation in plastic viscosity is too large for an accurate prediction of the flow rate.

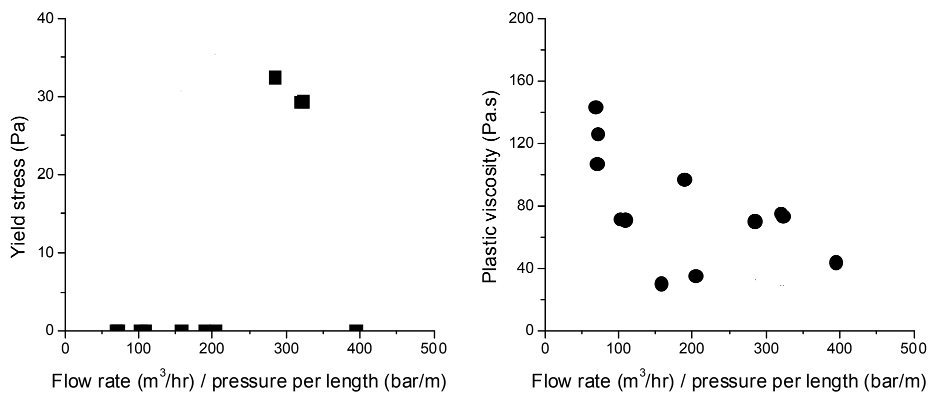

Figure 2: Relation between the flow rate and the rheological properties

Table 1 and Fig. 2 show that the rheological properties of concrete are inadequate for a quantitative prediction of pumping. For the best results, the lubricating layer should be taken into account.

There is no experimental way to measure the thickness of the lubricating layer or to determine how the rheological properties vary in relation to the thickness of the layer. The results of numerical analyses are used in this study to evaluate the formative role of SIPM on the lubricating layer and to estimate how the lubricating layer affects concrete pumping.

3 SIPM Analysis of the Flow of Concrete in a Pipe

3.1 SIPM

The rheological properties of concrete depend on the particle concentration of materials such as cement, sand, and gravel. The fact that the lubricating layer has a lower plastic viscosity and yield stress indicates that the particle concentration of the lubricating layer is lower than that of the concrete flowing in the pipe. SIPM helps explain this phenomenon [Phillips, Armstrong and Brown (1992)]. That is, the particles in concentrated suspensions subjected to an inhomogeneous shear stress migrate across the streamlines from regions with a high strain rate to regions with a low strain rate. The governing equation of SIPM for a Poiseuille flow was derived as follows [Phillips, Armstrong, and Brown (1992):Lam, Chen, Tan, Chai and Yu (2004)]

$$\frac{\partial \phi}{\partial t}+\frac{\partial (u_z\phi)}{\partial z}=\nabla\cdot\left\{a^2K_c\phi\nabla\left(\phi\ \frac{\partial u_z}{\partial r}\right)\right\}+\nabla\cdot\left\{K_\mu\phi^2a^2\frac{\partial u_z}{\partial r}\frac{\nabla\mu_{app}}{\mu_{app}}\right\}, \tag{2}$$

where φ is the particle concentration, t is the time, U_z is the velocity component in the flow direction, a is the particle radius, z is the flow direction, r is the radial direction, a is the particle radius, μ_{app} is the apparent viscosity of the concentrated suspension, and K_c and K_μ are dimensionless phenomenological constants. In Eq. (2), the particle flux is expressed as a balance between the effect of the spatially varying interaction frequency and the effect of the spatially varying viscosity. Fig. 3 schematically describes the balance of the particle migration between the two effects.

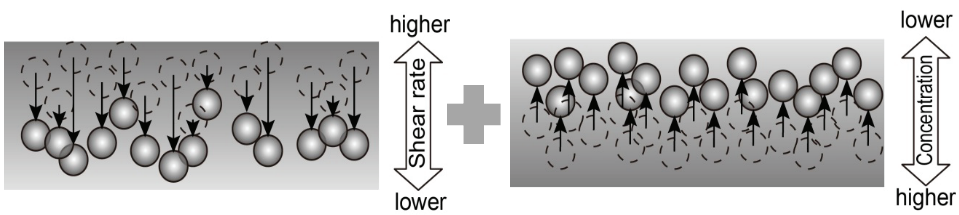

Figure 3: Schematic of SIPM

Fig. 4 shows the Bingham fluid model [Tattersall and Banfill (1983)], which is widely used to represent the rheology of concrete.

The apparent viscosity in Eq. (2) can be written as follows;

$$\mu_{app}=\mu_p+\frac{\tau_0}{\dot{\gamma}}, \tag{3}$$

where μ_p and τ_0 are the plastic viscosity and yield stress of the Bingham fluid model, respectively. Fresh concrete consists of three representative particles, each of which has a different scale of length: cement (micrometers) sand (millimeters) and gravel (centimeters). The plastic viscosity and yield stress are functions of the concentrations of those particles.

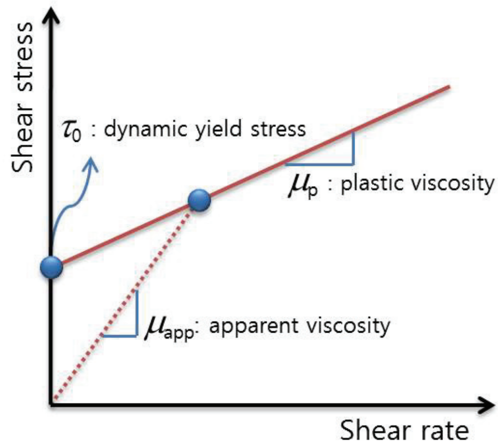

Figure 4: Bingham fluid model

3.2 *The particles of fresh concrete*

In this study, the profile of a concentration of each type of particle over a cross section of the pipe is calculated for the Poiseuille flow of concrete. Fig. 5 shows a schematic of how the different types of particles affect the rheological properties of a concrete mix. The concentrations of cement, sand and gravel represent the volume fraction of cement particles in cement paste, the volume fraction of sand particles in mortar, and the volume fraction of gravel particles in concrete, respectively. In other words, the concentration is not based on the volume fraction of each particle in the total volume of concrete; rather, the concentration is assumed to be the volume fraction of particles in the local region where the SIPM occurs. Because the particles are of a different scale, the migration of one type of particle does not affect the migration another type of particle.

The plastic viscosity and yield stress are derived from the following equations [Hafid et al. (2010); Chateau, Ovarlez and Trung (2008); Ferraris and Brower (2004)]

$$\mu_p = \mu_i \left(1 - \frac{\phi_{cem}}{\phi_{cem,c}}\right)^{-2.5\phi_{cem,c}} \left(1 - \frac{\phi_{sand}}{\phi_{sand,c}}\right)^{-2.5\phi_{sand,c}} \left(1 - \frac{\phi_{gravel}}{\phi_{gravel,c}}\right)^{-2.5\phi_{gravel,c}} \tag{4}$$

$$\tau_0 = \tau_i \sqrt{\frac{1-\phi_{cem}}{\left(1-\frac{\phi_{cem}}{\phi_{cem,c}}\right)^{2.5\phi_{cem,c}}}} \sqrt{\frac{1-\phi_{sand}}{\left(1-\frac{\phi_{sand}}{\phi_{sand,c}}\right)^{2.5\phi_{sand,c}}}} \sqrt{\frac{1-\phi_{gravel}}{\left(1-\frac{\phi_{gravle}}{\phi_{gravel,c}}\right)^{2.5\phi_{gravel,c}}}}, \tag{5}$$

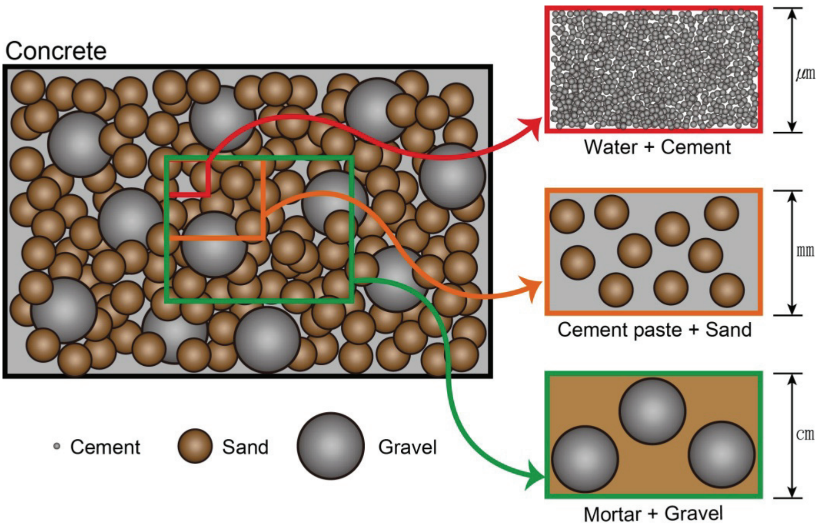

Figure 5: Concentrations of particles of different lengths

where ϕ_{cem} is the concentration of cement particles in cement paste; ϕ_{sand} is the concentration of sand particles in mortar; ϕ_{gravel} is the concentration of gravel in concrete; the subscript c of $\phi_{cem,c}$, $\phi_{sand,c}$, and $\phi_{gravel,c}$ is the maximum concentration of each of the particles and μ_i and τ_i are the plastic viscosity and yield stress at zero concentration, respectively.

3.3 Pipe modeling and analysis conditions

The flow of concrete in a pipe can be considered as a creeping flow because its viscosity is high and the velocity is too low to be affected by the inertial force of the particles. The conservation equations for a steady incompressible flow can be written as follows [Lam, Chen, Tan, Chai and Yu (2004)]:

$$\nabla \cdot \vec{u} = 0 \tag{6}$$

$$-\nabla p + \nabla \cdot \bar{\tau} = 0, \tag{7}$$

where $\vec{u}$ is the velocity vector, p is the hydrostatic pressure, and $\bar{\tau}$ is the stress tensor. Eqs. (6) and (7), which are used for axisymmetric flows, are expressed as follows in terms of cylindrical coordinates (r,θ,z):

$$\frac{\partial u_r}{\partial r} + \frac{u_r}{r} + \frac{\partial u_z}{\partial z} = 0 \tag{8}$$

$$-\frac{\partial p}{\partial r}+\frac{\partial \tau_{rr}}{\partial r}+\frac{\tau_{rr}}{r}+\frac{\partial \tau_{zr}}{\partial z}-\frac{\tau_{\theta\theta}}{r}=0 \tag{9}$$

$$-\frac{\partial p}{\partial z}+\frac{\partial \tau_{rz}}{\partial r}+\frac{\tau_{rz}}{r}+\frac{\partial \tau_{zz}}{\partial z}=0. \tag{10}$$

In Eqs. (9) and (10), τ_{rz} is identical to τ_{zr} because of symmetry. The stress tensor, $\bar{\tau}$, is simply expressed as follows:

$$\bar{\tau}=\mu_{app}\left(|\dot{\gamma}|,\phi_{cem},\phi_{sand},\phi_{gravel}\right)\bar{\dot{\gamma}}, \tag{11}$$

where $\bar{\dot{\gamma}}$ is the strain rate tensor and $|\dot{\gamma}|$ can be written as follows:

$$|\dot{\gamma}|=\left[\frac{1}{2}\left(\bar{\dot{\gamma}}:\bar{\dot{\gamma}}\right)\right]^{1/2}=\left[\frac{1}{2}\left(\dot{\gamma}_{rr}^2+\dot{\gamma}_{\theta\theta}^2+\dot{\gamma}_{zz}^2+\dot{\gamma}_{rz}^2\right)\right]^{1/2}. \tag{12}$$

The components of the strain rate tensor, $\bar{\dot{\gamma}}$, are given by the following:

$$\dot{\gamma}_{rr}=2\frac{\partial u_r}{\partial r},\quad \dot{\gamma}_{\theta\theta}=2\frac{u_r}{r},\quad \dot{\gamma}_{zz}=2\frac{\partial u_z}{\partial z},\quad \dot{\gamma}_{rz}=\dot{\gamma}_{zr}=\frac{\partial u_z}{\partial r}+\frac{\partial u_r}{\partial z}. \tag{13}$$

In Eq. (11), the apparent viscosity is a function of the strain rate and the concentrations of cement, sand and gravel as derived in Eqs. (3) to (5). For a pressure-driven pipe flow, the following conditions must be satisfied:

$$p=p(z),\quad u_z=u_z(r,z),\quad u_r<<u_z,\quad \frac{\partial}{\partial z}<<\frac{\partial}{\partial r}. \tag{14}$$

The conditions of Eq. (14) reduce Eqs. (8) to (10) to the following equations:

$$\frac{\partial p}{\partial z}-\frac{1}{r}\frac{\partial}{\partial r}\left(r\mu_{app}\frac{\partial u_z}{\partial r}\right)=0 \tag{15}$$

$$Q=2\pi\int_0^R r\cdot u_z\,dr, \tag{16}$$

where R is the radius of pipe and Q is the flow rate.

The concentration profile and the flow of concrete in the pipe were numerically calculated from the governing equations (2), (15), and (16). Eq. (2) was solved individually for three concentrations of cement, sand, and gravel particles. At the wall of the pipe, two boundary conditions were considered in the analysis: a non-slip condition and a zero particle flux through the wall [Lam et al.(2004)]. Thus,

$$\left\{K_c\phi\nabla\left(\phi\frac{\partial U_z}{\partial r}\right)+K_\mu\phi^2\frac{\partial U_z}{\partial r}\frac{\nabla\mu_{app}}{\mu_{app}}\right\}\cdot\vec{n}=0, \tag{17}$$

where $\vec{n}$ is the outer normal unit vector. The particle concentrations of cement, ϕ_{cem}, sand, ϕ_{sand}, and gravel, ϕ_{gravel}, were assumed to be uniform over the cross section of the pipe at the inlet. Thus,

$$\phi_{cem} = \phi_{cem,0}, \quad \phi_{sand} = \phi_{sand,0}, \quad \phi_{gravel} = \phi_{gravel,0} \text{ for } 0 \le r \le R \text{ at } z = 0, \tag{18}$$

where $\phi_{cem,0}$, $\phi_{sand,0}$, and $\phi_{gravel,0}$ are the initial concentrations of cement, sand, and gravel particles, respectively. Table 2 shows the mix proportions considered in the analysis: the proportion was used in the construction of Burj Khalifa. The initial concentration of each type of particle in the mix is also listed in Table 2. In Eq. (2), the parameters, K_c and $K_\mu$should be independent of the particle size, the concentration, and the shear rate, and the values of the parameters were set to 0.3 and 0.6, respectively [Phillips, Armstrong and Brown (1992)]. In Eqs. (4) and (5), the maximum concentrations, $\phi_{cem,c}$, $\phi_{sand,c}$, and $\phi_{gravel,c}$ were all set to 0.60 in accordance with the study of Ferraris and Brower (2004).

Table 2: Mix proportions and particle concentrations

	w/b	Water	Cement	Sand	Gravel
Mix proportions (kg/m^3)	35.6	172	484	731	914
Initial particle concentration (%)			40.1	50.3	36.2

Fig. 6(a) shows the two-dimensional axisymmetric modeling of the pipe. The total length of the pipe was 1.5 m. Fig. 6(b) shows part of the mesh the pipe.

The commercial computational fluid dynamics software [Fluent Inc. (2010)] was used to calculate the pipe flow. In addition, a subroutine program called User-Defined Scalar [Fluent Inc. (2010)] was coded to solve Eq. (2) for the concentrations of cement, sand and gravel. The subroutine was interlocked with the pipe flow analysis.

3.4 Parametric study

The purpose of the parametric analysis is to determine how the various factors or parameters influence the formation of the lubricating layer or, more specifically, how the parameters affect the thickness and rheological properties of the lubricating layer. The parametric study was performed with variations of the following important parameters: the plastic viscosity and yield stress at a zero concentration, the inlet pressure, the size of the gravel, the water-binder ratio, and the diameter

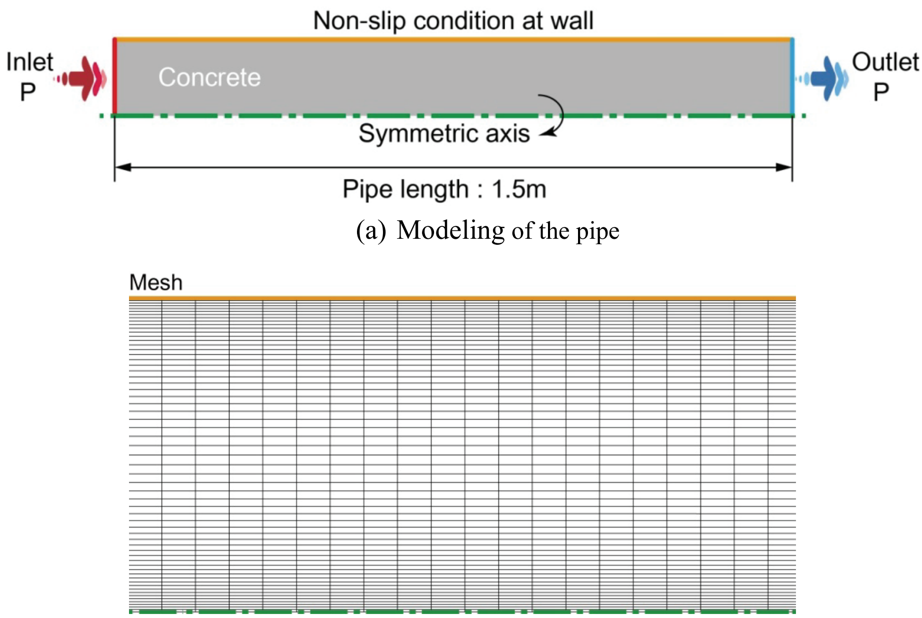

(a) Modeling of the pipe

(b) Mesh of the pipe

Figure 6: Pipe modeling and boundary conditions

of the pipe. Table 3 lists the variations of the parameters in detail, covering the practical range of each parameter.

The analysis was first performed for the reference values of the parameters listed in Table 3. Additional analyses were then performed as the parameters were varied one by one. For example, in analysis case C1, the plastic viscosity at a zero concentration was varied while the other parameters (reference values) were kept constant.

In the analyses, the particle concentration profile, the plastic viscosity and the yield stress profiles, and the shear rate and velocity profiles were obtained for a fully developed steady state.

4 Results and discussion

4.1 Particle concentrations

The concentration profiles calculated from the reference parameters of Table 3 are displayed in Fig. 7. The concentrations abruptly decrease near the wall of the pipe.

Table 3: Details of the parametric study

Parameters			Reference	Variation		Analysis case
Plastic viscosity at a zero concentration	μ_i	(Pa·s)	1.0	0.5	1.5	C1
Yield stress at a zero concentration	τ_i	(Pa)	10	5	15	C2
Inlet pressure	P_0	(kPa/m)	30	20	40	C3
Size of particles	a_{cem}	(μm)	12.5	12.5	12.5	C4
	a_{sand}	(μm)	625	625	625	
	a_{gravel}	(μm)	6000	3000	4000	
Water-binder ratio	*w/b	(%)	47	25	32	C5
Pipe diameter	D	(mm)	150	125		C6

* w/b=47%: $\phi_{cem,0}$ =40.1, $\phi_{sand,0}$ =50.3, $\phi_{gravel,0}$ =36.2

w/b=25%: $\phi_{cem,0}$ =57.3, $\phi_{sand,0}$ =42.6, $\phi_{gravel,0}$ =32.6

w/b=32%: $\phi_{cem,0}$ =49.8, $\phi_{sand,0}$ =46.3, $\phi_{gravel,0}$ =34.4

As the particle size increases, the concentration at the wall is reduced more; there is also an increase in the size of the region near the wall where the concentration is changing. Lower concentrations reduce the plastic viscosity and yield stress near the wall and induce a higher shear rate and velocity near the wall.

Figure 8 shows how the concentration profiles vary in relation to variation of the parameters listed in Table 3. In Fig. 8, the concentrations are expressed as normalized concentrations; these concentrations are relative to the maximum concentrations. In cases C1 and C2, the concentrations are not dependent on the plastic viscosity, μ_i, and the yield stress, τ_i, at zero concentration of Eqs. (4) and (5). In case C3, there is no change in concentration for different pressure levels. In case C4, when the particle size of gravel decreases, the minimum concentrations at the wall are almost constant, and the concentration profile of gravel particle moves toward to the wall. In case C5, the water-binder ratio varies from 47% to 25%. Table 3 lists the corresponding initial concentrations of cement, sand and gravel. A decrease in the

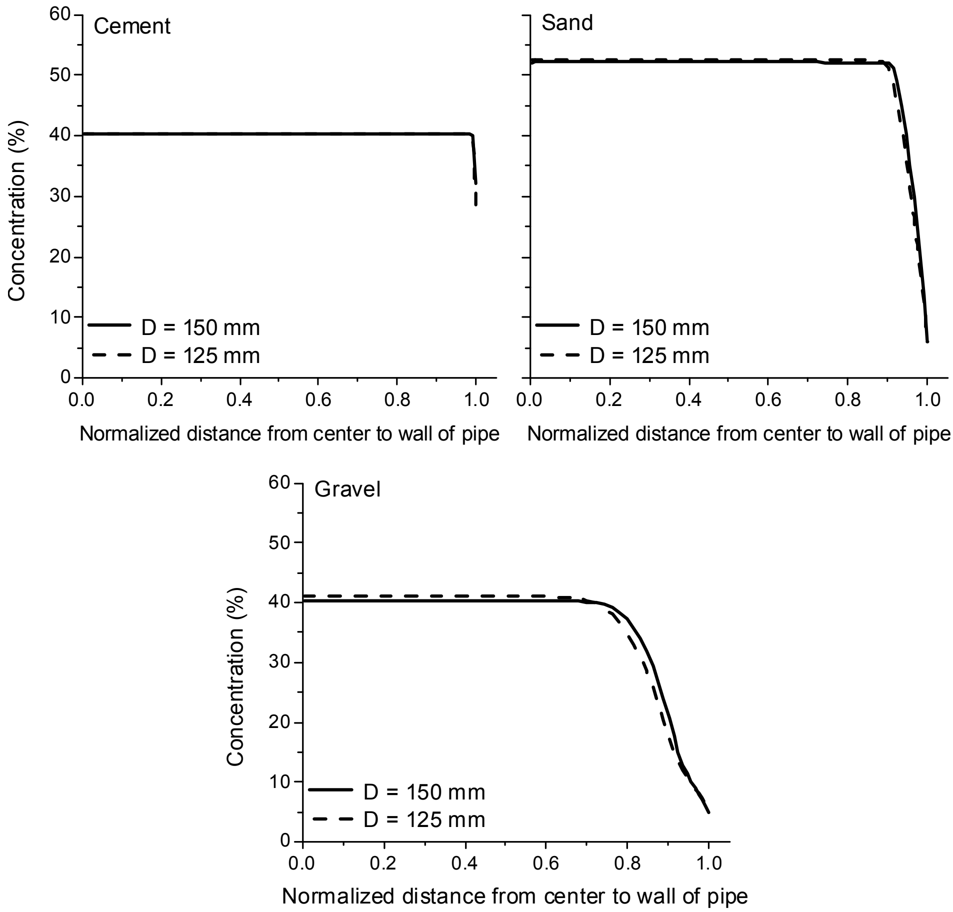

Figure 7: Concentration profiles calculated from the reference parameters

water-binder ratio seems to cause no apparent change in the concentration profile for cement, though the sand and gravel particles are definitely more concentrated near the wall. In the graph of case C6, the x-axis represents the normalized pipe radius. An increase in diameter of the pipe appears to cause no apparent change in the cement profile, though the sand and gravel particles are slightly more concentrated near the wall and the minimum concentration is almost the same.

4.2 Plastic viscosity and yield stress

Figs. 9 and 10 show how the plastic viscosity and yield stress over the cross section of the pipe vary in relation to the concentration profiles.

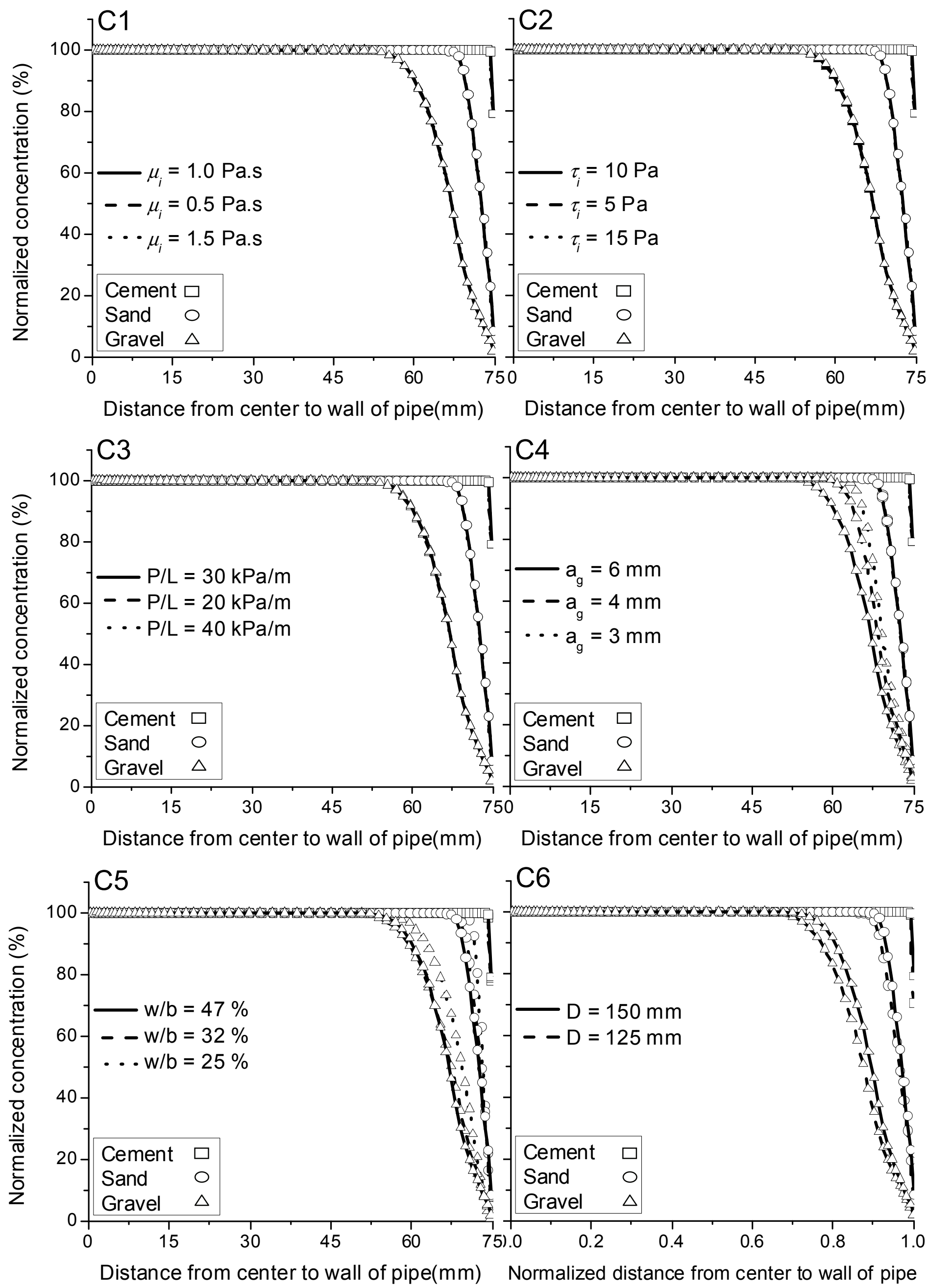

Figure 8: Concentration profiles for parametric variations

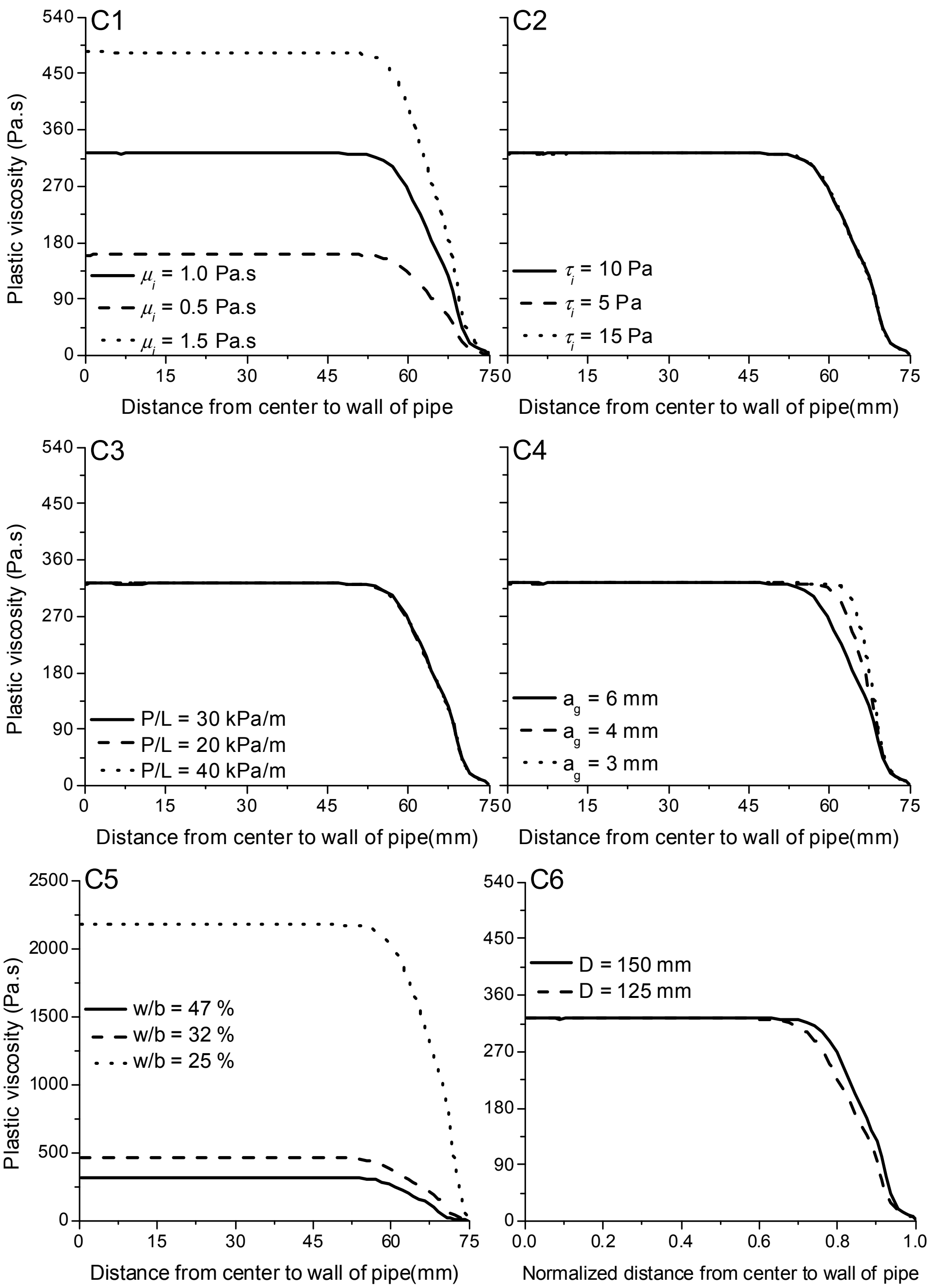

Figure 9: Plastic viscosity profiles for parametric variations

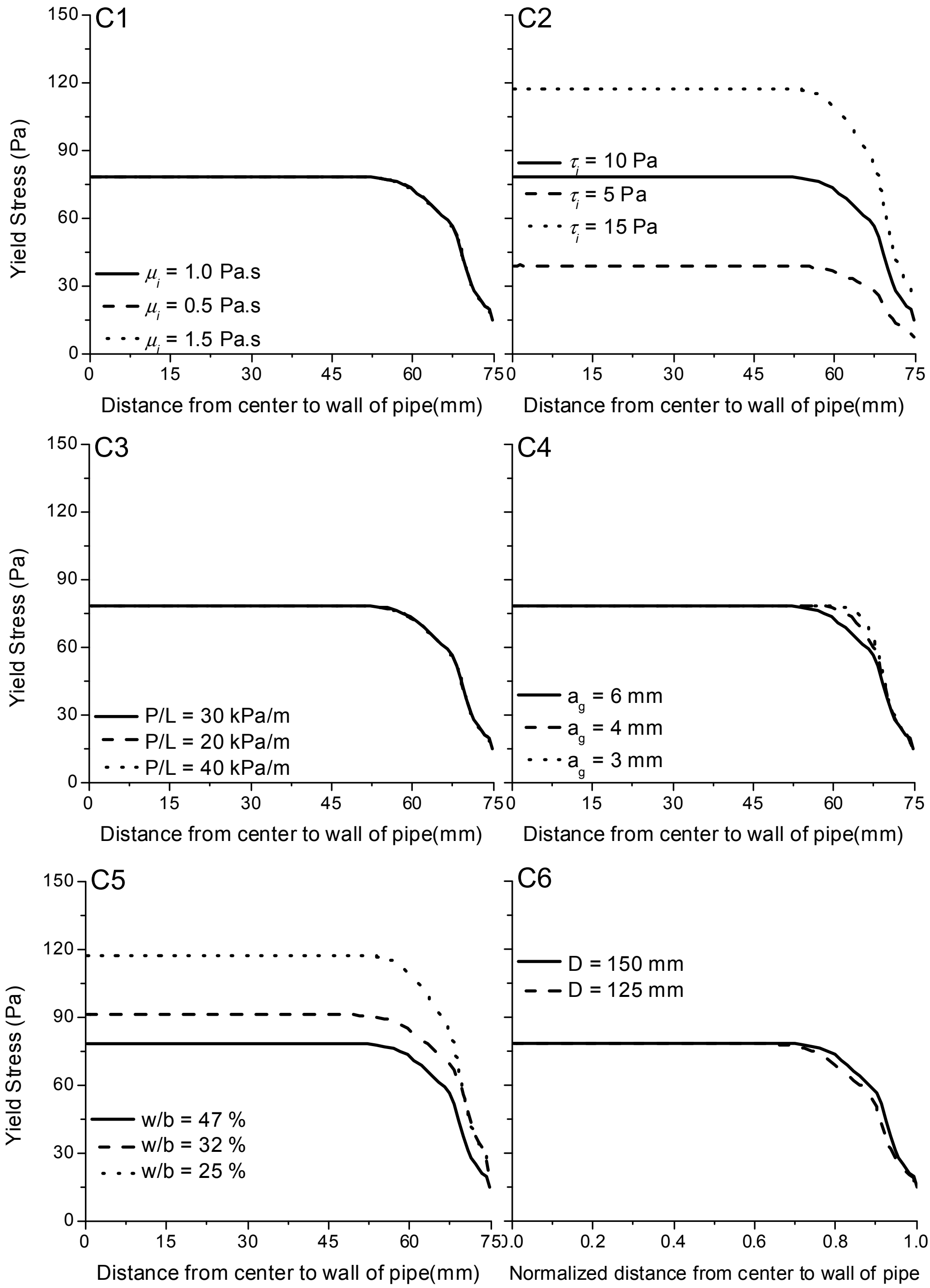

Figure 10: Yield stress profiles for parametric variations

In cases C1 and C2, the plastic viscosity shifts vertically as the plastic viscosity at zero concentration increases and does not depend on variations in the yield stress at zero concentration. In contrast, the yield stress profile remains constant while the plastic viscosity at zero concentration varies; and it moves upwards as the yield stress at zero concentration increases. In case C3, the plastic viscosity and yield stress profiles are independent of the pressure variations. In case C4, an increase in the gravel size causes no apparent change in the plastic viscosity and yield stress profiles within a distance of around 5 mm from the wall, though these profiles undergo a decrease at distances between 5 mm and 15 mm from the wall. As shown in case C5, the plastic viscosity and yield stress profiles shift vertically with variations in the water-binder ratio. In case C6, the profiles remain constant for a normalized pipe radius in the range of 0.95 to 1.00 but deviate slightly for a normalized pipe radius in the range of from 0.70 to 0.95.

4.3 Shear rate and velocity

As explained in Eq. (15), the shear rate and velocity profiles depend on the apparent viscosity, which is a function of the plastic viscosity and the yield stress. Figs. 11 and 12 show the results of the shear rate and velocity profiles obtained from the analyses. The lubricating layer is a region where the velocity sharply increases. Thus, the thickness of the lubricating layer can be determined from the velocity profile; and the average plastic viscosity and yield stress within the lubricating layer can be estimated from the results shown in Figs. 9 and 10.

The shear rate and velocity change steeply near the wall or in the lubricating layer but elsewhere are almost constant or change in a gradual manner. In cases C1 and C2, the shear rate and velocity in the lubricating layer depend strongly on the plastic viscosity at zero concentration but are not greatly influenced by variations in the yield stress at zero concentration.

In case C3, as shown in Figs. 11 and 12, the shear rate and velocity are proportional to the pressure level. This proportionality occurs because the shear stress is linearly proportional to the pressure level and because, as shown in Figs. 9 and 10, the plastic viscosity and yield stress profiles are independent of the pressure level.

In case C4, although the concentration, plastic viscosity and yield stress profiles depend on the gravel size, as seen Figs. 8, 9, and 10, the shear rate and velocity are almost constant even when the gravel size varies.

In cases C1, C2, C3, and C4, the thickness of the lubricating layer is about 5 mm from the wall. In case C5, a decrease in the water-binder ratio caused the lubricating layer to become thinner (that is, from a thickness of 5 mm to 1 mm).

In case C6, the shear rate profiles for the different diameters of the pipe are almost

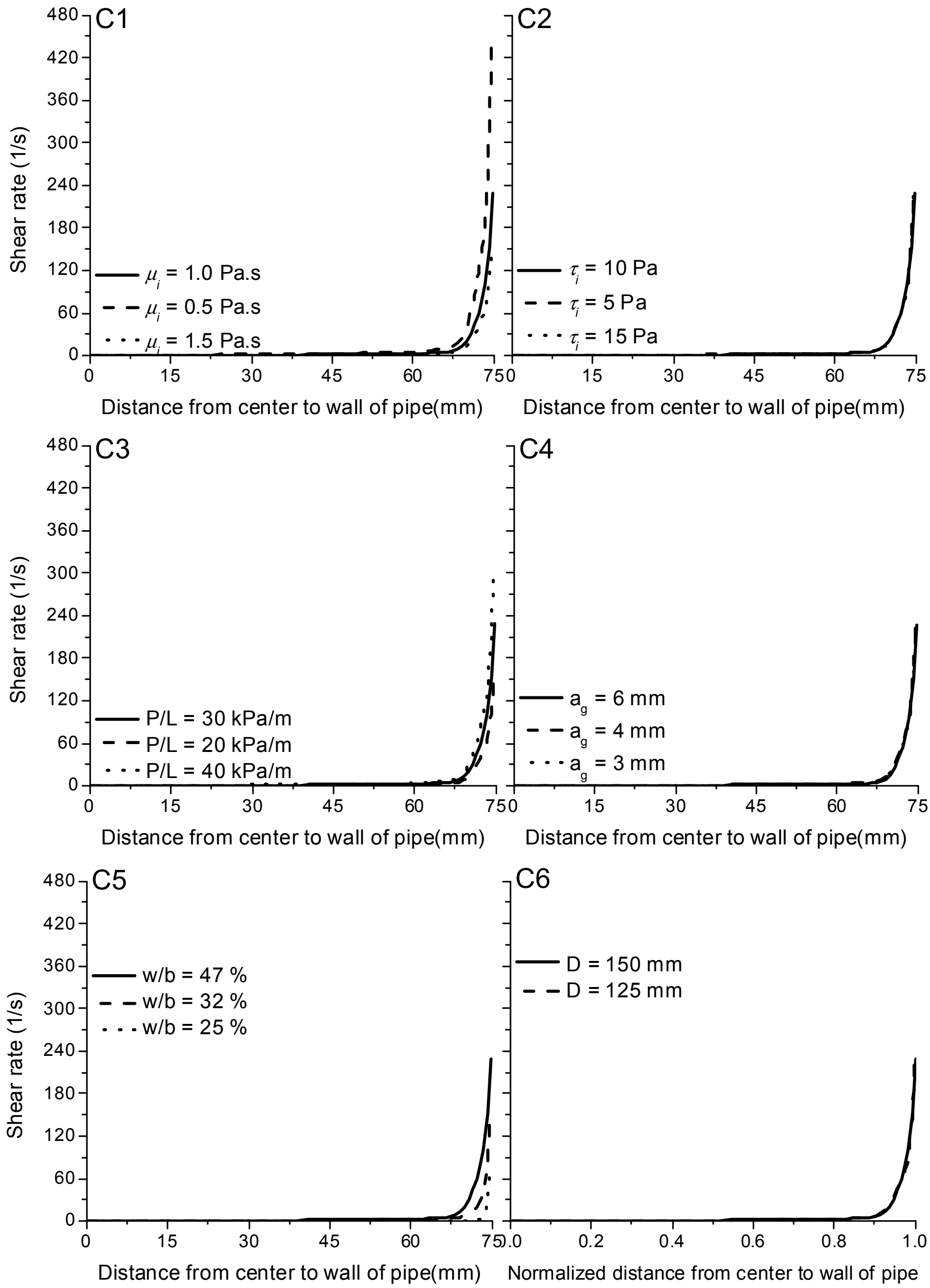

Figure 11: Shear rate profiles for parametric variations

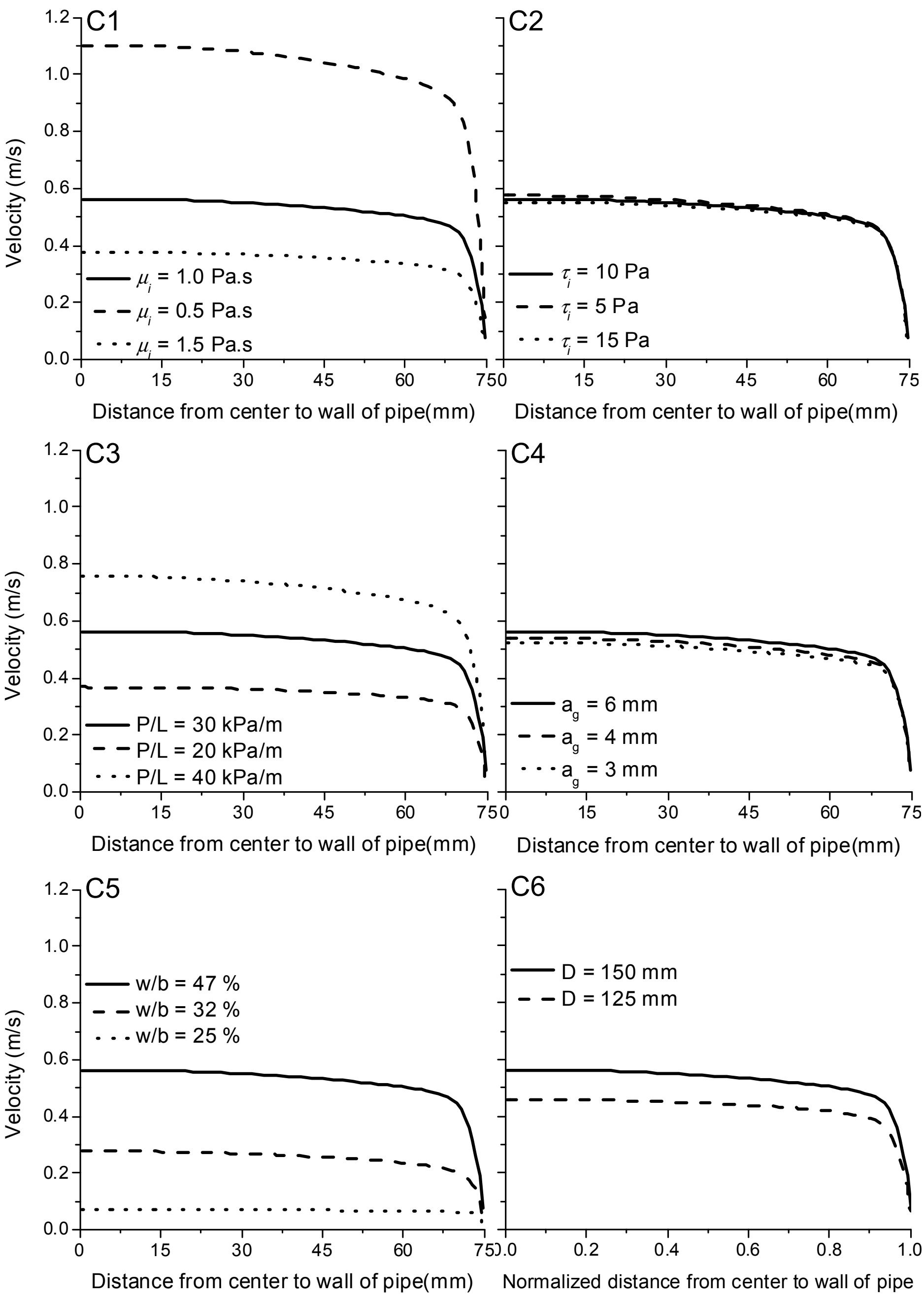

Figure 12: Velocity profiles for parametric variations

identical for a normalized pipe radius. The velocity profile is also higher for a larger diameter because the same inlet pressure per pipe length was applied to the pipes with a different diameter. The thickness of the lubricating layer seems to be around 7% of the normalized radius.

For every analysis case, the average plastic viscosity within the lubricating layer ranges from one-fifth to one-fifteenth of the plastic viscosity of the inner concrete, and the average yield stress of the lubricating layer is about one-fifth of the yield stress of the inner concrete.

5 Conclusion

This study describes a way of estimating the thickness and rheological properties of a lubricating layer that forms near the wall of a pipe in concrete pumping. Computational fluid dynamics was used to analyze a concrete flow in a pipe while consideration was given to the SIPM of cement, sand, and gravel particles. The analysis provides insight into how the concentration profile, the plastic viscosity and yield stress profiles, and the shear rate and velocity profiles vary in relation to the parametric variations that influence pumping. The following conclusions can be drawn from the analysis:

(1) The flow rate in a given pressure level and the pressure level required to the targeted flow rate cannot be predicted only with the plastic viscosity and yield stress of concrete measured from a concrete rheometer. The effect of the lubricating layer should be considered in any quantitative prediction of concrete pumping.

(2) The thickness of the lubricating layer varies in relation to the particle concentrations of cement, sand, and gravel, as well as the diameter of the pipe. The thickness of the lubricating layer ranges from about 1 mm to 5 mm.

(3) The average plastic viscosity in the lubricating layer ranges from one-fifth to one-fifteenth of the plastic viscosity of the inner concrete; and the mean value of the yield stress in the lubricating layer is about one-fifth of the yield stress of the inner concrete.

(4) The particle concentration profiles, the plastic viscosity profiles and the yield stress profiles are not dependent on the pressure level.

(5) The gravel size does not appear to affect the thickness of the lubricating layer or the rheological properties of the layer.

(6) Although the rheological properties differ for a given mix proportion or the initial concentrations of cement, sand and gravel, the thickness of the lubricating layer remains almost constant.

(7) The thickness of the lubricating layer varies in relation to the mix proportion.

The lubricating layer is thinner, for example, if the water-binder ratio is lower.

This study analyzes various parameters to estimate the thickness and rheological properties of a lubricating layer in a concrete pumping process. Although the study sheds light on the formation of the lubricating layer, its ability to predict concrete pumping capability is far from accurate. These days many different types of concrete are used in construction. Each type of concrete has different mix proportions and different rheological properties. It is important, therefore, to find a way of accurately measuring the rheological properties of the lubricating layer of concrete and to develop an analytical method of predicting the pumping especially with respect to the measured rheological properties for the lubricating layer.

Acknowledgement: This study was supported by the Samsung C&T Corporation.

References

Chapdelaine, F. (2007): Etude fondamentale et pratique sur le pompage du beton (in French). *Doctoral Thesis, University Laval*, Quebec, Canada.

Charkrabarty, A.; Cargin, T. (2008): Computational studies on mechanical and thermal properties of carbon nanotube based nanostructures. *CMC: Computers, Materials, & Continua*, vol. 7, pp. 167–190.

Chateau, X.; Ovarlez, G.; Trung, K.L. (2008): Homogenization approach to the behavior of suspensions of non-colloidal particles in yield stress fluids. *Journal of Rheology*, vol. 52, pp. 489-506.

Chun, S.-C.; Lee, S.-H.; Oh, B. (2010): Simplified design equation of lap splice length in compression. *International Journal of Concrete Structures and Materials*, vol. 40, pp. 63-68.

Ferretti, E.; Leo, A.D. (2008): Cracking and creep role in displacements at constant load: concrete solids in compression. *CMC: Computers, Materials, & Continua*, vol. 7, pp. 59-80.

Ferraris, C.F.; Brower, L.E. (2004): Comparison of concrete rheometers: international tests at MB (Cleveland OH, USA) in 2003. *National Institute of Standards and Technology Interagency Report*, NISTIR 7145.

Fluent Inc. (2010): FLUENT Ver. 12 , *Lebanon, NH: Fluent Inc*.

Hafid, H.; Ovarlez, G.; Toussaint, F.; Jezequel, P.H.; Roussel, N. (2010): Estimating measurement artifacts in concrete rheometers from MRI measurement on model materials. *Proceedings of SCC2010*, Motreal, Canada, pp. 127-137.

Kaplan, D.; Larrard, F.; Sedran, T. (2005): Design of concrete pumping. *ACI*

Materials Journal, vol. 102, pp. 110-117.

Kim, J.H.; Beacraft, M.W.; Kwon, S.H.; Shah, S.P. (2011): Simple analytical model for formwork design of self-consolidating concrete. *ACI Materials Journal*, vol. 108, pp. 38-45.

Kwon, S.H.; Zhao, Z.; Shah, S.P. (2008): Effect of specimen size on fracture energy and softening curve of concrete: Part II. Inverse analysis and softening curve. *Cement and Concrete Research*, vol. 38, pp. 1061-1069.

Kwon, S.H.; Shah, S.P.; Phung, Q.T.; Kim, J.H.; Lee, Y. (2010): Intrinsic model to predict formwork pressure. *ACI Materials Journal*, vol. 107, pp. 20-26.

Kwon, S.H.; Phung Q.T.; Park, H.Y.; Kim, J.H.; Shah, S.P. (2011): Effect of wall friction on variation of formwork pressure over time in self-consolidating concrete. *Cement and Concrete Research*, vol. 41, pp. 90-101.

Lam, Y.C.; Chen, X.; Tan, K.W.; Chai, J.C.; Yu, S.C.M. (2003): Numerical investigation of particle migration in Poiseuille flow of composite system. *Composite Science and Technology*, vol. 64, pp. 1001-1010.

Nghia, T.T.; Chu, I.-Y.; Kim, J.-J. (2010): Critical compressive strain of concrete under a long-term deformation effect Part I. Experiment. *International Journal of Concrete Structures and Materials*, vol. 40, pp. 89-96.

Ngo, T.T.; Bennacer, R.; Cussigh, F. (2010): Use of tribometer to estimate interface friction and concrete boundary layer composition during the fluid concrete pumping. *Construction and Building Materials*, vol. 24, pp. 1253-1261.

Phillips, R.J.; Armstrong, R.C.; Brown, R.A. (1992): A constitutive equation for concentrated suspensions that account for shear-induced particle migration. *Physics of Fluids*, vol. A4, pp.30-40.

Sohn, Y.S.; Lee, J.H.; Lee, S.H. (2010): Application of ultra-high-strength concrete for high-rise building. *Proceedings of the 7th International Symposium on Advancement of Cement and Concrete Industries*, Seoul, Korea, pp. 105-125.

Tattersall, G.H.; Banfill, P.F.G. (1983): The rheology of fresh concrete. *Pitman Advanced Publishing Program*, pp. 53-67.

Zhao, Z.; Kwon, S.H.; Shah, S.P. (2008): Effect of specimen size on fracture energy and softening curve of concrete: Part I. Experiments and fracture energy. *Cement and Concrete Research*, vol. 38, pp. 1049-1060.